AMERICAN UNIVERSITY OF BEIRUT

MAROUN SEMAAN FACULTY OF ENGINEERING & ARCHITECTURE

American University of Beirut

Maroun Semaan Faculty of Engineering and Architecture

MECH 510 Project

Group Progress Report

Fall 2022

Project Title: Thermosyphon Loop

Group & Disciplines

Name	ID
Aya Sabe Ayoun	202000855
Jihad Jundi	202000646
Carl Tamerian	202001294
Omar Shaaban	202001660

Contents

1 System Description

[1] explains that a thermosyphon loop is a passive heat exchange system that is usually based on natural convection. It circulates a fluid, usually liquids or volatile gases, without the requirement of a mechanical pump. A thermosyphon loop can either be open or close looped; however, in this paper, the closed loop thermosyphon will be taken into account.

A closed-loop thermosyphon is typically arranged in a vertical position, and the circulation of the fluid inside occurs due to the difference in temperature from the hot and cold side that makes way for changes in density. The warmer fluid on one side of the thermosyphon is less dense than the cooler fluid on the other side. This will induce a motion where the warmer fluid "floats" above the cooler fluid and the cooler fluid "sinks" below the warmer fluid creating the natural flow of the fluid inside the thermosyphon. A good thermosyphon system has very little hydraulic resistance so that the fluid can easily flow under the relatively low pressure produced by natural convection.

2 Introduction

In this paper, a closed loop thermosyphon system as seen in figure (1) is under study, where the fluid is considered to be water, the material is considered to be copper, the warm side is heated with a constant surface temperature T_s, and the cooler side is equipped with fins to enhance the natural convection with the ambient and as a result increase the induced flow rate.

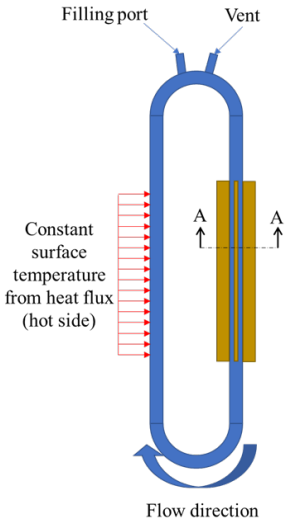

Figure 1: Thermosyphon Loop [2]

In addition, the fins are added in modules, where each module consists of 6

fins with dimensions as can be seen in figure (2)

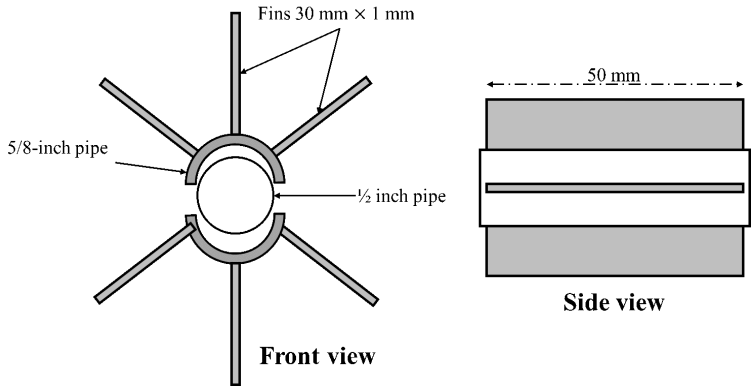

Figure 2: Fins setup [2]

3 Literature Review

Fundamental applications of thermosyphon systems are found in [3–5]. Palm et al. consider different fluids in order to optimize the performance of thermosyphon systems. This performance was based on the thermos-physical properties, heat transfer coefficient, and effects on the environment. Ammonia seemed to be the best choice due to its thermodynamic properties despite its toxic nature [6]. Thermosyphons can be used in many different applications and in multiple configurations. The cold side can be cooled using water or air. Water is used more often because of its higher conductivity and capacity to be used as a dual-phase, where the density difference is higher between liquid and vapor phases [7].

The previous work done by Alizadeh et al. [8] focuses on enhancing the performance of a longitudinal fin-assisted thermosyphon loop by varying the heat input, filling ratio, number of fins, and coolant flow rate. Their study revealed that increasing the coolant flow rate and filling ratio enhances the overall efficiency of the system. Moreover, they found out that the thermal resistance could be decreased by increasing the number of fins, heat input, and filling ratio.

Cataldo et al. [7] evaluated the performance of a closed-loop thermosyphon system using R1234ze as the coolant in the cooling of a transistor module through natural and forced convection. They found that natural convection mode represents an optimal cooler for power electronics since it needs no energy input for heat removal. They also found that using forced convection improves the thermal resistance of the transistor due to the enhanced cooling provided.

Although Cataldo et al. proved the capability of utilizing thermosyphon

systems as coolers for power electronics, they did not confirm the possibility of using thermosyphons as energy storage systems. In our project, we shall develop a numerical model of a thermosyphon loop, optimize it and evaluate this possibility.

The method of enhancement of heat and mass transfer of a tall fin using cycloid thermosyphon loop is found in [9]. Tan relied on using an aluminum fin integrated with the thermosyphon loop since it can improve the thermal heat dissipation from the heat source that has light weight and high efficiency features due to the charge resulting from the charge phase working fluid. In his experiment, he tested a cellular thermosyphon fin (CET fin) and a cycloid thermosyphon fin (CYT fin).

[9] results show that the CYT fin always results in a better temperature distribution and improves the average thermal resistance by around 10.1%. Tan also found that the presence of a vapor cavity in the blind channels can lead to the enhancement of the condensation and the promotion of the liquid level on the heating side. While experimenting to validate our model, we can test this to validate the results of Tan.

After proposing and studying a total of four optimized configurations based on tested CYT fins, the results show that the optimum configuration with the four vapor zones allocated in one partition can posses 8.7% higher level liquid than that of the original CYT fin.

4 Numerical Model

A flowchart representing the algorithm is represented in the Figure (3).

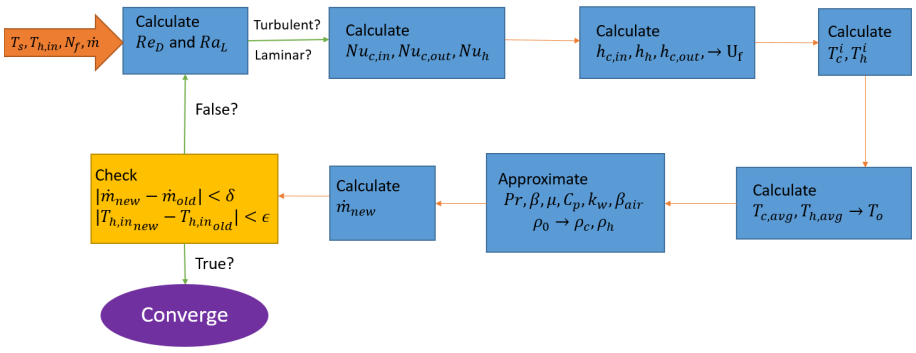

Figure 3: Pseudo-code of the Numerical Model

Using Table A6 from [10], we related Pr, μ, C_p, K_w, and ρ all to temperature T using linear regression applied using Excel considering that $T \in [20, 100]$. The following relations were obtained:

$$
\begin{aligned}
Pr &= -0.0568 * T + 22.351 \\
\mu &= -8 * 10^{-6} T + 0.0032 \\
C_p &= 9 * 10^{-6} T^2 - 0.0055 T + 5.0226 * 10^3 \\
K_w &= 0.0009 T + 0.3353 \\
\rho &= -0.003 T^2 + 1.4574 T + 824.96
\end{aligned} \tag{1}
$$

The values of (1) were initialised at the initial guess of $T_{h,in}$.

We considered

$$\beta_{air} = \frac{1}{\frac{T_{amb} + T_c avg}{2}} \tag{2}$$

But for the first iteration, $T_c avg$ was taken to be equal to $T_{h,in}$ to initialise the loop.

We also imposed the condition that the temperature leaving the cooling region is equal to that entering the heating region considering that the pipe bare surface is adiabatic.

$$T_{c,o} = T_{h,in} \tag{3}$$

On the heating side, the dominant form of heat transfer is internal convection. The convective heat transfer coefficient can be obtained through the Nusselt number, whose formula depends on the flow regime. The flow regime could be determined by evaluating the Reynolds Number given by:

$$Re = \frac{4\dot{m}}{P\mu} \tag{4}$$

The following equations are used to evaluate the value of the convective heat transfer coefficient h

$$N_{uc} = \begin{cases} 3.66 & \text{if } Re \leq 2300 \\ 0.0265 Re^{4/5} Pr^{0.3} & \text{if } Re > 2300 \end{cases} \tag{5}$$

$$N_{uh} = \begin{cases} 3.66 & \text{if } Re \leq 2300 \\ 0.0243 Re^{4/5} Pr^{0.4} & \text{if } Re > 2300 \end{cases} \tag{6}$$

The friction factor is also computed using the following equations to later obtain the value of the new mass flowrate.

$$\begin{cases} f = \frac{64}{Re} & \text{if } Re \leq 2300 \\ \frac{1}{\sqrt{f}} = -2 \log(\frac{\frac{e}{d}}{3.7} + \frac{2.51}{Re_D \sqrt{f}}) & \text{if } Re > 2300 \end{cases} \tag{7}$$

Now the value of h for the internal flow of water can be calculated on the cold and hot side:

$$h_H = \frac{Nu_h K_w}{D_p} \tag{8}$$

$$h_{Ci} = \frac{Nu_c K_w}{D_p} \tag{9}$$

Now, we can find T_h using equation (10).

$$T_h = T_s - (T_s - T_h) e^{\frac{-h_H P X_h}{\dot{m} C_p}} \tag{10}$$

where X_h represents the discretized length of the heated side.
To get the average value of a function, the following formula is adopted:

$$\frac{1}{b-a} \int_a^b f(x)dx \tag{11}$$

In addition, the value of the integral is approximated by the sum of N rectangles with an equal width Δx distributed in the range [a,b].

$$\int_a^b f(x)dx = \sum_{n=1}^{N} f(n)\Delta x \tag{12}$$

To find T_{havg}, we have to integrate T_h over the length of the heating section in the thermosyphon loop. We get:

$$T_{havg} = \frac{1}{H} \int_0^H Th(x)dx = \frac{1}{H} \sum_{n=1}^{N} Th(n)\Delta x \tag{13}$$

For the natural convection occurring at the external cooling side, we obtain:

$$Gr = \frac{9.81\beta_{air}|T_{cavg} - T_{amb}|(N_f * 50 * 10^{-3})^3}{\nu_{air}^2} \tag{14}$$

$$Ra = GrPr_{air} \tag{15}$$

$$Nu_{co} = \begin{cases} 0.59Ra^{1/4} & \text{if } Ra \leq 10^9 \\ 0.1Ra^{1/3} & \text{if } Ra > 10^9 \end{cases} \tag{16}$$

Consequently, we can find:

$$h_{Co} = \frac{Nu_{co} K_{air}}{N_f * 50 * 10^{-3}} \tag{17}$$

The fin efficiencies have to be calculated to obtain the U-value, which will be used in determining the temperature distribution.
The finned and total areas of the fins could be represented by the following equations:

$$\begin{aligned} A_f &= N_f(2 * 30 * 50 * 10^{-6} * 6) \\ A_o &= A_f + N_f(P - 6 * 10^{-3}) * 50 * 10^{-3} \end{aligned} \tag{18}$$

To compute the efficiencies of the fins:

$$\eta_f = \frac{\arctan\left(30 * 10^{-3} m\right)}{30 * 10^{-3} m} \tag{19}$$

with

$$m = \sqrt{\frac{2h_{Co}}{10^{-3} K_{copper}}} \tag{20}$$

$$\eta_o = 1 - (1 - \eta_f)\frac{A_f}{A_o} \tag{21}$$

The U-value can be obtained through the following relations:

$$UA_f = (\frac{1}{h_i A_i} + \frac{1}{\eta_o h_o A_o})^{-1} \tag{22}$$

$$U_f = \frac{UA_f}{A_f} \tag{23}$$

Finally, the temperature distribution at the finned (cooling) side can be obtained:

$$T_c = T_{amb} - (T_{amb} - T_h) * exp(\frac{-2 * 6 * 30 * 10^{-3} X_c U_f}{\dot{m} C_p}) \tag{24}$$

where X_c represents the discretized length of the finned side

Similarly to equations [(11)-(13)], to get T_{cavg} we have to integrate T_c over the length of the thermosyphon that is finned and is experiencing natural convection. We get:

$$T_{cavg} = \frac{1}{H_f} \sum_{n=1}^{N} Tc(n)\Delta x \tag{25}$$

The average temperature across the whole loop is calculated as the average of the hot and cold side temperatures by:

$$T_o = \frac{T_{cavg} + T_{havg}}{2} \tag{26}$$

To will be used for the reevaluation of the thermophysical properties from (1) and (2) Consequently, we can get the densities of water at the cooling and heating sides respectively:

$$\rho_c = -0.003 T_{cavg}^2 + 1.4574 T_{cavg} + 824.96 \tag{27}$$

$$\rho_h = -0.003T_{havg}^2 + 1.4574 * T_{havg} + 824.96 \tag{28}$$

Finally, we can obtain the mass flow rate using equation (29):

$$\dot{m} = \sqrt{\frac{9.81|\rho_c - \rho_h|H * 2 * \rho A_{cs} * 2D_p}{L_t f}} \tag{29}$$

Also, we impose the following condition to satisfy the adiabatic bare surface condition

$$T_{h,in} = T_{c,out} \tag{30}$$

For our algorithm to converge given a certain set of values for N_f and T_s with an initial guess for $\dot{m}$ and $T_{h,in}$, the following convergence criteria must be satisfied:

1. The absolute difference between the mass flow rates obtained at iterations i and $i+1$ must be less than a specified tolerance.
2. The absolute difference between the temperatures at the inlet of the heated side obtained at iterations i and $i+1$ must be less than a specified tolerance.

5 Optimization

5.1 Objective Function

The objective function for the cost is shown in equation (31).

$$LCC = 150(USD/m^2) * A_f(m^2) + \sum_{j=1}^{12} \frac{0.3(USD/kWh) * Q(kW) * (20 * 8)(h)}{(1 + 0.0067)^j} \tag{31}$$

To find Q, we use energy balance on the hot part of the U-tube.

$$Q_h(kW) = 10^-3 * h_H(W/m^2.K)A(m^2)(T_s - T_{h,avg}) \tag{32}$$

It should be noted that $A_f = N_f * 6 * 50 * 30 * 10^-6 = 0.009N_f$
Therefore, after simplification, our cost objective function becomes:

$$LCC = 1.35 * N_f + \sum_{j=1}^{12} \frac{48 * 10^{-3} * h_H PH(T_s - T_{h,avg})}{(1.0067)^j} \tag{33}$$

5.2 Constraints

After iterating the mathematical model in section 4 for various values of T_s and N_f, multi-variable regression was performed on MATLAB to obtain $\dot{m}$, T_{cavg},

T_{havg}, and h_H as a function of T_s and N_f

$$\begin{aligned}
\dot{m}(kg/s) &= -0.00086618 - 4.0304 * 10^{-6} T_s + 2.4422 * 10^{-8} T_s^2 \\
&+ (-6.6765 * 10^{-5} - 4.9464 * 10^{-7} T_s + 2.8121 * 10^{-9} T_s^2) N_f \\
&+ (-3.6277 * 10^{-6} + 4.6695 * 10^{-8} T_s + -1.3234 * 10^{-10} T_s^2) N_f^2 \\
T_{cavg}(K) &= (2.5974 + 0.99057 T_s + 4.6845 * 10^{-7} T_s^2) \\
&+ (6.021 - 0.024819 T_s + 1.564 * 10^{-5} T_s^2) N_f \\
&+ (-0.29418 + 0.0015591 T_s - 1.9251 * 10^{-6} T_s^2) N_f^2 \\
T_{havg}(K) &= (4.3383 + 0.98404 T_s + 6.4927 * 10^{-6} T_s^2) \\
&+ (4.5568 - 0.016783 T_s + 4.9266 * 10^{-6} T_s^2) N_f \\
&+ (-0.22922 + 0.0012198 T_s - 1.4939 * 10^{-6} T_s^2) N_f^2 \\
h_H(W/(m^2 K)) &= (102.7897 + 0.22485 T_s + 4.6706 * 10^{-5} T_s^2) \\
&+ (-0.28775 + 0.004837 T_s - 1.3045 * 10^{-5} T_s^2) N_f \\
&+ (0.048527 - 0.00035445 T_s + 6.4776 * 10^{-7} T_s^2) N_f^2
\end{aligned} \tag{34}$$

By substituting (34) into (33), we get the objective function in terms of the design variables N_f and T_s. Consequently, We optimize the design variables such that $\dot{m}$ and T_{cavg} reach a minimum desired value, so they are considered as constraints where:

$$\begin{cases} \dot{m} & \geq 2g/s \\ T_{cavg} & \geq 318.15K \end{cases} \tag{35}$$

In order to ensure that the water does not evaporate and reach the saturation region, the temperature of the hot surface is restricted to below $100°C$. In addition, it is taken that the surface temperature is greater than ambient temperature by at least $5°C$

The length of the pipe is equal to $0.75m$ and the length of a single module of fins is $50 * 10^{-3} m$. So, the maximum number of fin modules we can install is $\frac{0.75}{50*10^{-3}} = 15$. Thus, we obtain the range of the design variables as follows:

$$\begin{cases} 303.15 & \leq T_s(K) \leq 373.15 \\ 1 & \leq N_f \leq 15 \end{cases} \tag{36}$$

5.3 Results

The penalty function in correlation with cyclic coordinate method is implemented using MATLAB, and the optimal values of N_f and T_s are obtained. The penalty function takes in the objective function (31) and the constraints (35) and returns the optimized values of the design variables up to a specified tolerance.

The optimal values were found to be:

$$\begin{cases} T_s & = 373.15K \\ N_f & = 10.67 \approx 11 \end{cases} \tag{37}$$

6 Experimental Results

6.1 Determination of inputs

In order to validate our results for the optimum T_s and N_f, we were asked to reevaluate both optimum values for the following constraints:

$$\begin{cases} \dot{m} & \geq 1.5g/s \\ T_{cavg} & \geq 308.15K \end{cases} \tag{38}$$

and the optimal values were found to be:

$$\begin{cases} T_s & = 370.15K \\ N_f & = 4 \end{cases} \tag{39}$$

These values will be used in the experiment.

6.2 Experimental Results

In the experiment, 4 modules of fins were added to the cold side and heated the hot surface to a constant temperature of $97.2°C$. The following measurements:

$$\begin{cases} T_c(1) = 91.2°C \\ T_c(end) = 86.8°C \\ T_{Amb} = 24°C \\ \dot{Q} = 167.043W \end{cases} \tag{40}$$

In order to validate our results we would like to check the the mass flow rate for the experiment. Thus, the mass flow rate is calculated by energy balance on the cold side of the pipe as follows:

$$\dot{m}C_{pair}[T_c(1) - T_c(end)] = dotQ] \tag{41}$$

where,

$$\begin{cases} T_c(1) = 91.2°C \\ T_c(end) = 86.8°C \\ \dot{Q} = 167.043W \end{cases} \tag{42}$$

$$\dot{m} = \frac{dotQ}{C_p * [Tc(1) - Tc(end)]} = \frac{167.043}{4200 * [91.2 - 86.8]} = 0.009kg/s = 9g/s \tag{43}$$

6.3 Discussion

The calculated experimental flow rate of $9g/s$ and the numerically achieved one of $1.5g/s$ vary greatly with a percentage difference calculated as shown:

$$\%\Delta\dot{m} = \frac{\dot{m}_{exp} - \dot{m}_{num}}{\dot{m}_{num}} * 100 = \frac{9 - 1.5}{1.5} * 100 = 500\% \tag{44}$$

This percentage difference is very significant, and this can be attributed to multiple experimental errors and assumptions taken in the modeling. Such as:

- The ambient temperature in the room is $24°C$, while the one assumed in the model is at $25°C$.
- The parts of the thermosyphon assumed to be perfectly insulated and adiabatic are not in reality. This results in heat losses to the ambient air not taken into account in the model.
- The parts of the cold side of the thermosyphon with no fin modules were not insulated, resulting in heat losses to the outside.
- Radiation losses through the fins and the tube were not taken into account in the model, resulting in lower heat losses with the environment in the numerical model.
- The experimental measurements were not taken while the system was at steady state. They were taken during the transient increase of temperature. Thus, resulting in different measures than those found through the numerical model where steady state is assumed.
- The fin modules were not attached properly. This can result in high contact resistance between the tube and the fins, inhibiting the heat transfer from the cold side to the ambient air.
- The measurement of T_s was done on 1 point of the hot surface side, rather than checking for constant temperature through out the tube. Therefore, the temperature might not be equal to 97.2 throughout. This will result in differences between the numerical and experimental results.
- The length of the thermosyphon was not consistent with the one used for the modeling, since it was only possible to attach maximum of 5 fin modules only instead of 15.
- The purity of the copper is not ensured from the fin modules. Thus, the conductivity used in the numerical model might be significantly different to the actual conductivity.
- The given heat flow of the strip heater does not necessarily only transfer heat to the tube surface. There might be losses to the ambient due to convection and radiation.

- Human error in taking the measurements might also have caused significant errors in the temperature measurements.
- The linear approximations to multiple parameters in the model may not be accurate as many of the correlations are not linear. This will cause variance between the experimental and numerical results.

  Therefore, the resulting error might be due to many different errors and assumptions that were not met in the experiment. However, mistakes in the numerical model might be contributing to additional errors. It cannot be confirmed without further experimentation in more controlled conditions.

7 Appendix

7.1 Geometric Relations

- $P = \pi D_p(m)$
- $A_{cs} = \frac{\pi D_p^2}{4}(m^2)$

7.2 Constants

- $D_p = 12.7 * 10^{-3}(m)$
- $H = 0.75(m)$
- $L_t = 2.44(m)$
- $K_{copper} = 401(W/mK)$
- $\rho_{air} = 1.614(Kg/m^3)$
- $C_{pair} = 1.007 * 10^3(J/kgK)$
- $\nu_{air} = 15.89 * 10^{-6}(m^2/s)$
- $K_{air} = 26.3 * 10^{-3}(W/mK)$
- $\alpha = 22.5 * 10^{-6}(m^2/s)$
- $Pr_{air} = 0.707$

7.3 Terminology

- D_p: Pipe's diameter.
- H:Pipe's vertical leg length .
- L_t: Pipe's total length.

- P: Pipe's perimeter.
- K_{copper}: Thermal conductivity of copper.
- A_{cs}: Pipe's cross sectional area.
- ρ_{air}:density of air.
- ρ_{hot}:density of water on hot side.
- ρ_{cold}:density of water on cold side.
- C_{pair}: specific heat capacity of air.
- ν_{air}: Dynamic Viscosity of air.
- Pr_{air}: Prandtl number of air.
- N_f: Number of fin modules.
- A_f: Area of total fins.
- H_f: height of total fins.
- Δx: height differential.
- A_o: Total area (finned + bare surface).
- K_w: Thermal conductivity of water.
- T_h: Hot side's temperature.
- T_hav: Cold side's average temperature.
- β_{air}: volumetric thermal expansion coefficient of air.
- T_c: Cold side's temperature.
- T_{cav}: Cold side's average temperature.
- Nu_h: Nusselt's Number of fluid for hot side.
- Nu_c: Nusselt's Number of fluid for cold side.
- h_H: Convective heat coefficient for the hot side.
- h_{Ci}: Convective heat coefficient for the cold inner side.
- h_{Co}: Convective heat coefficient for the cold outer side.
- η_f: Efficiency of the fins.
- η_o: Total efficiency of N fins.
- m: mass of the fluid.(g)

- Gr: Grashof Number.
- T_s: Temperature of the surface on the hot side.
- Ra: Rayleigh Number.
- Re_D: Reynold's Number.
- f: Friction factor.
- e/d: Relative roughness of the pipe
- $\dot{m}$: mass flow rate of water.
- Q_h: heat flow needed to maintain surface temperature on the hot side.
- ν_{air}: kinematic viscosity of air.
- μ: dynamic viscosity of water.
- α: thermal diffusivity of air.
- LCC:life cycle assessment.

References

[1] "Thermosiphon," Oct 2022.

[2] J. P. Harouz, "Word document on moodle," Nov 2022.

[3] H. Shabgard, M. J. Allen, N. Sharifi, S. P. Benn, A. Faghri, and T. L. Bergman, "Heat pipe heat exchangers and heat sinks: Opportunities, challenges, applications, analysis, and state of the art," *International Journal of Heat and Mass Transfer*, vol. 89, pp. 138–158, 2015.

[4] D. Jafari, A. Franco, S. Filippeschi, and P. Di Marco, "Two-phase closed thermosyphons: A review of studies and solar applications," *Renewable and Sustainable Energy Reviews*, vol. 53, pp. 575–593, 2016.

[5] C. Chan, E. Siqueiros, J. Ling-Chin, M. Royapoor, and A. Roskilly, "Heat utilisation technologies: A critical review of heat pipes," *Renewable and Sustainable Energy Reviews*, vol. 50, pp. 615–627, 2015.

[6] B. r. Palm and R. Khodabandeh, "Choosing working fluid for two-phase thermosyphon systems for cooling of electronics," *J. Electron. Packag.*, vol. 125, no. 2, pp. 276–281, 2003.

[7] F. Cataldo and J. R. Thome, "Experimental evaluation of the thermal performances of a thermosyphon cooling system rejecting heat by natural and forced convection," *Applied Thermal Engineering*, vol. 127, pp. 1404–1415, 2017.

[8] M. Alizadeh and D. Ganji, "Heat transfer characteristics and optimization of the efficiency and thermal resistance of a finned thermosyphon," *Applied Thermal Engineering*, vol. 183, p. 116136, 2021.

[9] Z. Tan, K. Duan, W. Xiu, X. Liu, Y. Wang, Q. Wang, and W. Chu, "Enhancement mechanism on heat and mass transfer of tall fin with cycloid thermosyphon loop," *International Journal of Heat and Mass Transfer*, vol. 198, p. 123432, 2022.

[10] F. P. Incropera, D. P. DeWitt, T. L. Bergman, A. S. Lavine, *et al.*, *Fundamentals of heat and mass transfer*, vol. 6. Wiley New York, 1996.